Dissipation-induced photonic-correlation transition in waveguide-QED systems

Zihao Chen, Yao Zhou, and Jung-Tsung Shen

Phys. Rev. A **96**, 053805 — Published 3 November 2017

DOI: 10.1103/PhysRevA.96.053805

Dissipation-Induced Photonic Correlation Transition in Waveguide QED Systems

Zihao Chen, Yao Zhou, and Jung-Tsung Shen*

Department of Electrical and System Engineering,

Washington University in St. Louis, Missouri 63130, USA

Abstract

We computationally study the effects of dissipations on correlated two-photon transport in waveguide quantum electrodynamic systems. We show that in the dissipative regime, the two-photon correlation signatures remain prominent even when the two-photon transport can be described by a single-photon picture. Moreover, by varying the dissipations, the photonic correlation can have an induced transition from bunching to antibunching, and vice versa, depending on the input quantum state.

* jushen@wustl.edu

Dissipations, resulting from the interplay between the physical system of interest and its ambient environment, are ubiquitous in all quantum nanophotonic systems [1–3]. One of the central goals in quantum nanophotonics is to generate photonic entanglement via atom-mediated photon-photon interactions [4–6]. In general, dissipations are considered deleterious that undermine photonic entanglement and impair photon transport (*e.g.,* total transmissions and reflections in one-dimensional systems). On the other hand, from the perspective of microscopic scattering, photonic dissipations are manifestations of photon leakages from the system of interest to the external environment. For initially entangled photons in the system, the entanglement should persist even after some of the photons are scattered out of the system (perhaps shared with other degrees of freedom in the environment). Conventionally, it is convenient to discuss the dynamics of the states that are restricted to the system only, and phenomenologically parametrize the effects of photon leakages by a set of few parameters. By doing so, it is obvious that photon transport is degraded by the dissipations. However, it is not clear, as *a priori*, how photonic entanglement is affected by dissipations. In this article, we computationally study the effects of dissipations on the photonic entanglement and the photon transport in waveguide quantum electrodynamic (wQED) systems. We confirm that when the dissipation increases, the transport metrics quickly degrade and exhibit no correlation signatures. Nonetheless, our results also reveal that even in this dissipative regime, the photons are still correlated (bunched or antibunched). That is, the correlation persists even when the transport metrics are described by a single-photon picture. Moreover, by varying the dissipations, the photon correlation can have a crossover from bunching to antibunching, and vice versa, depending on the input quantum state.

To begin with, we describe the wQED systems of interest. We focus on three fundamental configurations that are building blocks for more complicated systems: Fig. 1(a), a single two-level atom (in practice, the atom can be a genuine atom [7, 8], a superconducting qubit [9], or a quantum dot [10]); Fig. 1(b), a two-level atom coupled to a single-mode cavity [11, 12]; and Fig. 1(c), a two-level atom coupled to a ring-resonator [13, 14]. Each basic configuration is further coupled to a single-mode photonic waveguide. For each configuration, photons are injected into the waveguide from the left and, after scattering, the photonic correlation is numerically determined.

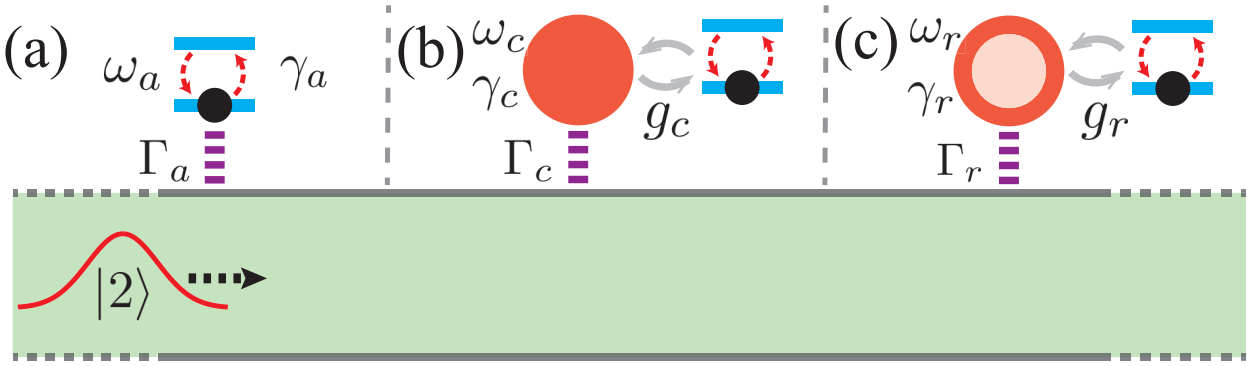

FIG. 1. Schematics of three wQED configurations of interest. (a) Single-atom case. (b) Atom-cavity case. (c) Atom-ring-resonator case. For each configuration, Γ is the decay rate into the waveguide. ω denotes the resonant frequency. γ is the intrinsic dissipation rate. g represents the coupling strength between the atom and the resonator. The subscripts a, c, and r denote the atom, cavity, and the ring-resonator, respectively. $|2\rangle$ denotes the incoming two-photon Fock state.

Single-atom configuration. The Hamiltonian describing the system of Fig. 1(a) is

$$\begin{aligned}\frac{H_a}{\hbar} = \int dx \Big(& c_R^\dagger(x)(-iv_g\partial_x)c_R(x) + c_L^\dagger(x)(iv_g\partial_x)c_L(x) \\ & + V_a\delta(x)\left[(c_R^\dagger(x)+c_L^\dagger(x))a_g^\dagger a_e + a_e^\dagger a_g(c_R(x)+c_L(x))\right]\Big) \\ & + (\omega_e - i\gamma_a)a_e^\dagger a_e + \omega_g a_g^\dagger a_g,\end{aligned} \tag{1}$$

where $c_R^\dagger(x)$ ($c_R(x)$) denotes the creation (annihilation) operator for a right-moving photon at position x. $c_L^\dagger(x)$ and $c_L(x)$ are analogously defined for a left-moving photon. $a_g^\dagger$ (a_g) is the creation (annihilation) operator of atomic ground state with energy $\hbar\omega_g$. $a_e^\dagger$, a_e, and ω_e are similarly defined for the excited state. $\omega_a \equiv \omega_e - \omega_g$ is the atomic transition frequency. v_g is the group velocity in the waveguide, and V_a is the atom-photon coupling ($V_a^2/v_g \equiv \Gamma_a$ is the atomic decay rate into the waveguide) [15]. γ_a is the atomic dissipation rate.

Here, we discuss how dissipations are incorporated by γ_a. For photon leakages, the external environment can be characterized into two scenarios. On one hand, the external environment contains an excitable medium (reservoir), thereby resulting in secondary photon scattering and absorptions by the medium. On the other hand, the environment can be non-excitable, and is described by photonic propagating channels. It has been shown that the photonic dissipations in both cases can be parametrized by a single parameter $-i\gamma_a$ in the atomic transition frequency [16, 17]; and the photonic dynamics of the combined system (system + environment) can be described by a reduced Hamiltonian (including $-i\gamma_a$) and

a restricted eigen-state (omitting the degrees of freedom in the reservoir or propagating channels). The restricted two-photon state is

$$|\Phi_a(t)\rangle = \Big(\int dx \sum_{j=R,L} e_j(x,t) c_j^\dagger(x) e^{-i\omega_e t} a_e^\dagger a_g + \iint dx_1 dx_2 \sum_{j,l=R,L} \phi_{jl}(x_1,x_2,t) e^{-i\omega_g t} \frac{c_j^\dagger(x_1) c_l^\dagger(x_2)}{\sqrt{2}} \Big) |\varnothing\rangle. \tag{2}$$

$|\varnothing\rangle$ is the vacuum state that has no waveguided photons, and the atom is in the ground state. $e_{R(L)}$ denotes the single-photon probability amplitude wherein one photon is absorbed by the atom and the other waveguided photon is moving to the right (left). ϕ_{RL} denotes the two-photon probability amplitude for the RL branch wherein one photon is moving to the right and the other to the left. ϕ_{RR}, ϕ_{LR}, and ϕ_{LL} are similarly defined (see Appendix A for the equations of motion to describe the two-photon transport dynamics).

To numerically determine the two-photon transport and the correlations, a two-photon Fock state is injected from the left. The incoming Fock state is an uncorrelated two-photon product state wherein each photon is resonant with the atom, and has a Gaussian waveform $\phi(x) = 1/(2\pi\sigma^2)^{1/4} \exp[-(x-x_o)^2/4\sigma^2 + i\omega_o x/v_g]$ ($\omega_o = \omega_a$ is the center frequency). The numerical initial condition is $\phi_{RR} = \phi_{in} = \phi(x_1)\phi(x_2)$ at $t = 0$. Here, $\sigma\Gamma_a/v_g = 15$ so that the photon has a narrow bandwidth $\Gamma_a/30$ ($x_o \approx -3.6\sigma$ is the initial position of the photon, and has no direct relevance of numerical results). The equations of motion are obtained from the Schrödinger Equation $i\hbar\partial_t|\Phi_a\rangle = H_a|\Phi_a\rangle$, which are numerically evolved to obtain the full spatiotemporal dynamics of the system (see Ref. [18] for details). In particular, such a numerical procedure yields, after scattering, the two-photon transmitted (ϕ_{RR}), two-photon reflected (ϕ_{LL}), and one-transmitted-one-reflected (ϕ_{RL} and ϕ_{LR}) wavefunctions, which provide complete information on the two-photon transport and correlations. We note that such an approach is also applicable to a weak coherent state input (see Ref. [18]).

Transport. After scattering, the photon transport properties are characterized by three quantities, T_2 (both photons are transmitted), R_2 (both reflected), and TR (one transmitted, the other reflected), respectively. T_2 is numerically evaluated by the two-photon transmitted flux $\iint dx_1 dx_2 |\phi_{RR}(x_1,x_2)|^2$. R_2 and TR are similarly defined. We visualize the transport properties by representing the triplet (T_2, R_2, TR) as a point in a three-dimensional plot (Fig. 2(a)). When γ_a varies, the triplet traces out a curve $\mathcal{C}$ (blue curve, the arrow indicates the direction of the increasing γ_a). To obtain deeper insight on the photon correlation, we

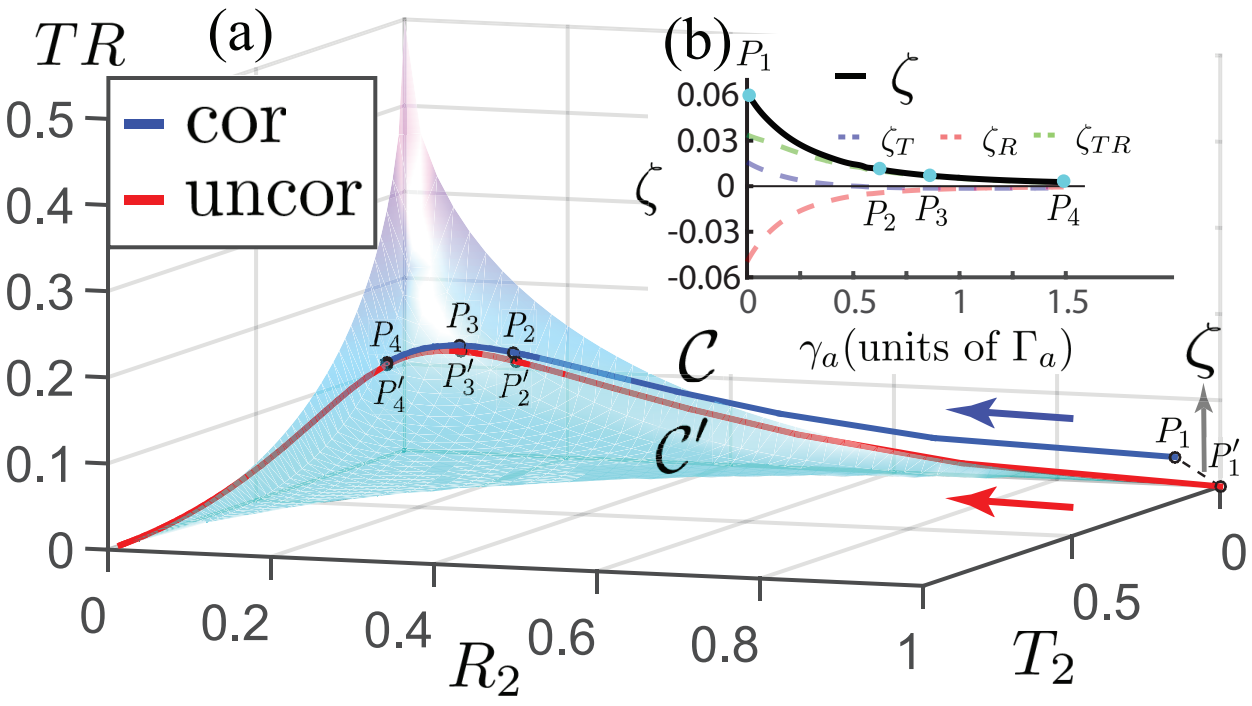

FIG. 2. Visualization of the two-photon transport metrics in the dissipative single-atom case. (a) Trajectory for correlated ($\mathcal{C}$) and uncorrelated ($\mathcal{C}'$) transport properties when varying γ_a. The points P_1, P_2, P_3, and P_4 on $\mathcal{C}$ represent the cases when $\gamma_a/\Gamma_a = 0,\ 0.62,\ 0.85,$ and 1.5, respectively. The primed points denote the corresponding points on $\mathcal{C}'$. (b) ζ, ζ_T, ζ_R and ζ_{TR} as a function of γ_a.

also plot the trace of the triplet based upon the single-photon picture. From the single-photon picture, the two-photon transport is the joint probability of the transports of two independent photons. Specifically, the uncorrelated two-photon transport is given by $T_2 = T_1^2, R_2 = R_1^2, TR = 2T_1R_1$, where T_1 and R_1 are single-photon transmission and reflection coefficients, respectively $(T_1, R_1) = ((\gamma_a/\Gamma_a)^2/(1+\gamma_a/\Gamma_a)^2, 1/(1+\gamma_a/\Gamma_a)^2)$. When varying γ_a, the triplet of the uncorrelated two-photon transport traces out a curve $\mathcal{C}'$ (red curve). It can be shown that $\mathcal{C}'$ lies on a surface because the constraint $\sqrt{T_2}+\sqrt{R_2}+\sqrt{2TR} = 1$ holds $\forall\ \gamma_a/\Gamma_a$ (noting that $\mathcal{C}$ does not lie on this surface). By definition, any point representing a scattering process that does not lie on $\mathcal{C}'$ indicates a two-photon correlation.

For a given γ_a, the transport properties of the correlated and uncorrelated systems are represented by P and P', respectively. For example, P_1 and P_1' describe the case for $\gamma_a = 0$. We now define the distance ζ between the two curves as the distance of two corresponding

TABLE I. Numerical metrics of scattered photons in RR and LL branches in the dissipative single-atom case.

$\frac{\gamma_a}{\Gamma_a}$	$\zeta(\gamma_a)$	$T_{2,cor}(\%)$	$g^{(2)}_{RR}(0)$	S_{RR} [a]	$R_{2,cor}(\%)$	$g^{(2)}_{LL}(0)$	S_{LL} [a]
0	0.062	1.6	85	B	95	0.025	A
0.62	0.011	2.1	0.98	B	14	0.062	A
0.85	0.0071	4.3	0.0039	A	8.3	0.08	A
1.5	0.0027	12.7	0.51	A	2.5	0.13	A

[a] S represents the photon statistics, which can be bunching (B) or antibunching (A).

point for the same γ_a, $\zeta \equiv \sqrt{\zeta_T^2 + \zeta_R^2 + \zeta_{TR}^2}$, where $\zeta_T = T_{2,cor} - T_{2,uncor}$, and ζ_R, ζ_{TR} are similarly defined. Fig. 2(b) plots ζ as a function of γ_a. As expected, ζ monotonically decreases and approaches to zero rapidly when γ_a increases. For example, when $\gamma_a = 1.5\Gamma_a$, ζ degrades to only 2.7×10^{-3}. Thus, for large dissipations, the two-photon transport metrics essentially exhibit no correlation signatures, and indeed can be predicted from a single-photon picture.

Correlation. Here, we study the effects of dissipations on photonic correlation by examining the second-order correlation function $g^{(2)}(\tau)$. Numerically, $g^{(2)}(\tau) = |\phi(x_m, x_m + v_g\tau)|^2 / \int dx' |\phi(x', x_m)|^2 \int dx' |\phi(x', x_m + v_g\tau)|^2$, where x_m is a reference position (see Ref. [18]). In Fig. 3(a), we plot the probability density ($|\phi|^2$) of the scattered photons for the $\gamma_a = 0$ case (see [19] for the animations of the scattering processes). $|\phi_{RR}|^2$ for two transmitted photons in Quadrant I (RR branch) is localized along $x_1 = x_2$, indicating photonic bunching because two photons tend to be collocated at the same spatial point [20]. We find numerically that $T_{2,cor} \approx 1.6\%$ while the single-photon picture gives $T_{2,uncor} = 0$. The numerically computed $g^{(2)}_{RR}(\tau)$ (red curve in Fig. 3(a)) is peaked at $\tau = 0$ ($g^{(2)}_{RR}(0) \approx 85 \gg 1$), confirming the bunching behavior. In Quadrant III, $|\phi_{LL}|^2$ for two reflected photons (LL branch) is depleted along $x_1 = x_2$, and $g^{(2)}_{LL}(\tau)$ has a dip at $\tau = 0$ (black curve, $g^{(2)}_{LL}(0) \approx 0.025 \ll 1$), both of which confirm the antibunching phenomenon.

We now examine the effects of dissipations by scanning γ_a in the range of $[0, 1.5\Gamma_a]$. We first focus on the RR branch. When γ_a increases, the two transmitted photons remain bunched while the bunching quality degrades as $g^{(2)}_{RR}(0)$ decreases. For example, when $\gamma_a \approx 0.62\Gamma_a$, $g^{(2)}_{RR}(\tau)$ still exhibits a peak at $\tau = 0$ and $g^{(2)}_{RR}(0) \approx 1$ (Fig. 3(b)). When γ_a is further

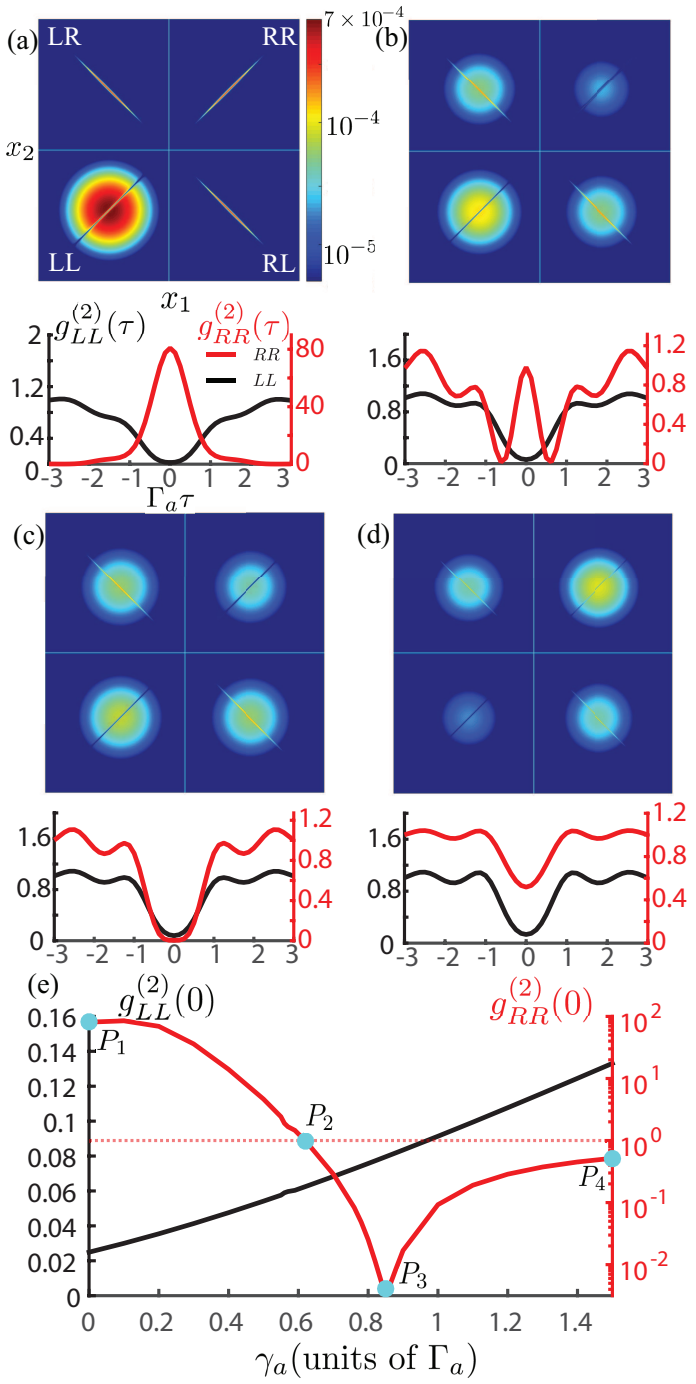

FIG. 3. Numerical results of the photonic correlations in the dissipative single-atom case. (a) Upper: probability density of the scattered photons for $\gamma_a = 0$. (a) Lower: $g^{(2)}(\tau)$ of the RR (red curve, right) and the LL (black curve, left) branches for $\gamma_a = 0$. (b) $\gamma_a = 0.62\Gamma_a$. (c) $\gamma_a = 0.85\Gamma_a$. (d) $\gamma_a = 1.5\Gamma_a$. (e) $g^{(2)}_{RR}(0)$ (red curve, right) and $g^{(2)}_{LL}(0)$ (black curve, left) for varying γ_a. The P points correspond to the cases in (a)-(d), respectively, which are the same as in Fig. 2.

increased to $\approx 0.85\Gamma_a$, the peak of $g^{(2)}_{RR}(\tau)$ at $\tau = 0$ disappears and a dip emerges, indicating that the photon statistics has a crossover, and now exhibits a strong antibunching signature ($g^{(2)}_{RR}(0) \approx 0$, Fig. 3(c)) [19]. Two transmitted photons remain antibunched when γ_a is further increased throughout the scanning range while the antibunching quality degrades as $g^{(2)}_{RR}(0)$ elevates and approaches to 1. Fig. 3(d) plots the results for the $\gamma_a = 1.5\Gamma_a$ case. For the LL branch, we find that two reflected photons remain antibunched throughout the scanning range so that no crossover occurs. Fig. 3(e) plots $g^{(2)}_{RR}(0)$ and $g^{(2)}_{LL}(0)$ as a function of γ_a, and Table I provides further numerical metrics. Here, we emphasize that when the correlation transition occurs (Fig. 3(c)), the transport metric ζ already significantly degrades to 7.1×10^{-3}, essentially agreeing with the single-photon picture. Thus, the information of photonic correlation is beyond that of the transport metric. In addition, we note that in the dissipative regime (Fig. 3(b)-(d)), $|\phi_{RR}|^2$, $|\phi_{RL}|^2$, and $|\phi_{LR}|^2$ spread out to off-diagonal regions. Such a photonic halo effect has been reported in Ref. [21].

In addition to the resonant Gaussian pulse, we have further investigated other cases of uncorrelated inputs (including the detuned Gaussian pulse and the two-sided exponentially decaying pulse, see Appendix A for details). The results indicate that for all uncorrelated two-photon input cases examined, the crossover occurs only in the RR branch from bunching to antibunching. A potential candidate to observe the photonic correlation transition is the superconducting circuit platform [22]. It has been reported that the tunability of the dissipation of the qubit can be realized by changing the resistance in the circuit [23].

Atom-cavity configuration (Fig. 1(b)). When the cavity is coupled to the atom, for the same resonant two-photon Gaussian input ($\omega_a = \omega_c = \omega_o$ and $\Gamma_c/g_c = 1$), the two transmitted photons (described by $|\phi_{RR}|^2$) and two reflected photons (described by $|\phi_{LL}|^2$) exhibit antibunching and bunching statistics, respectively [24]. We now investigate the photon correlations when varying the atomic dissipation (γ_a) and the cavity dissipation (γ_c) (see Appendix B for the equations of motion). The numerical results are plotted in Fig. 4. For the pure atomic dissipation case ($\gamma_c = 0, \gamma_a/g_c \in [0, 1.5]$), the statistics of $|\phi_{LL}|^2$ has a crossover from bunching to antibunching (black solid curve), and the statistics of $|\phi_{RR}|^2$ remains antibunching (not plotted) throughout the scanning range. For the pure cavity dissipation case ($\gamma_a = 0, \gamma_c/g_c \in [0, 1.5]$), the statistics of $|\phi_{LL}|^2$ remains bunching (black dashed curve) while the statistics of $|\phi_{RR}|^2$ (not plotted) remains antibunching throughout the scanning range, and no correlation transitions occur. For the case when both dissipations are present

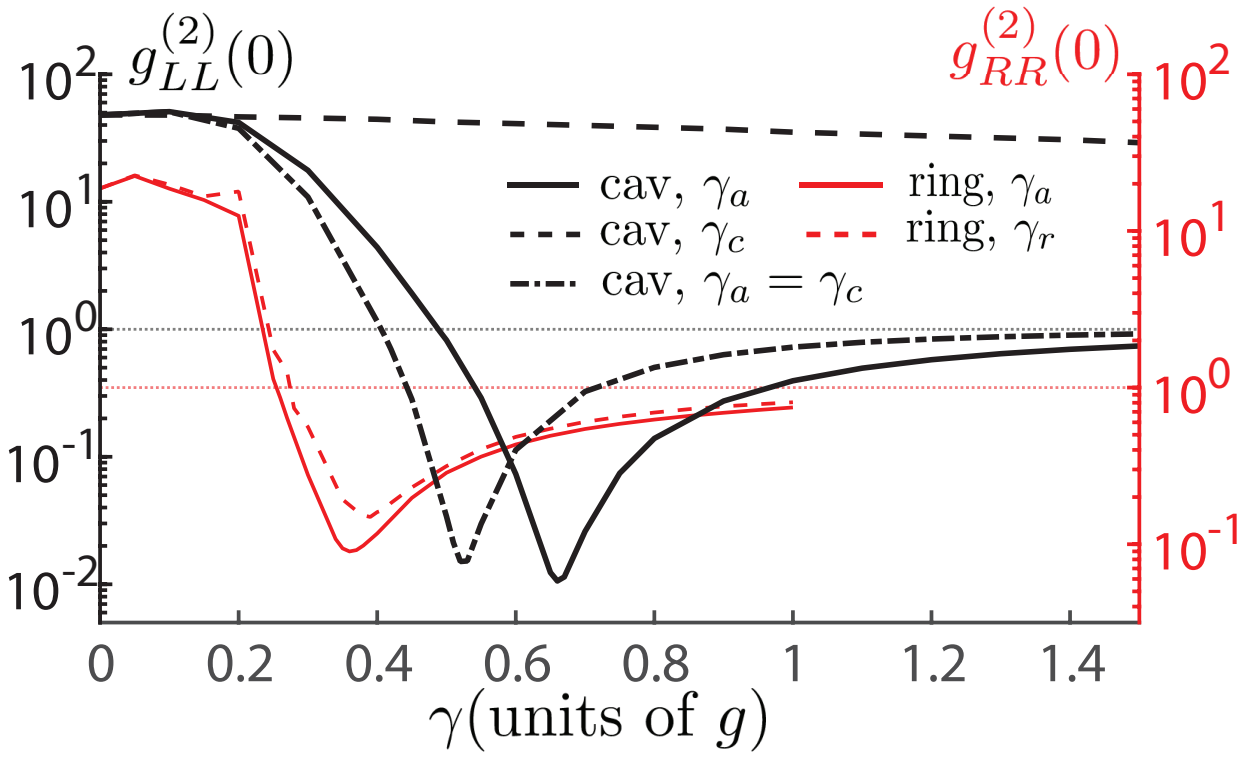

FIG. 4. Photonic correlations for varying dissipation rates in the dissipative atom-cavity (black curves, left) and the dissipative atom-ring-resonator (red curves, right) cases.

and equal ($\gamma_a/g_c = \gamma_c/g_c \in [0, 1.5]$), the statistics of $|\phi_{LL}|^2$ has a crossover from bunching to antibunching (black dashed-dot curve) while the statistics of $|\phi_{RR}|^2$ remains antibunching throughout the scanning range (not plotted). Numerically, we find that the correlation transitions only occur when the atomic dissipation $\gamma_a \neq 0$. We have also investigated the scenarios when $\Gamma_c/g_c \neq 1$ but varies within the range $[0.1, 5]$, and identify qualitatively the same correlation transition criteria.

Atom-ring-resonator configuration (Fig. 1(c)). When a ring-resonator is coupled to the resonant atom ($\omega_a = \omega_r$ and $\Gamma_r/g_r = 0.35$), the transmission spectrum exhibits three dips [25]. When a two-photon Gaussian input is operating at the left dip frequency (which can result in a large atomic excitation [25]), the two transmitted photons (described by $|\phi_{RR}|^2$) and two reflected photons (described by $|\phi_{LL}|^2$) exhibit bunching and antibunching statistics, respectively [21]. We now investigate the photon correlations when varying the atomic dissipation (γ_a), and the resonator dissipation (γ_r) (see Appendix C for the equations of motion). As shown in Fig. 4, for both the pure atomic dissipation case ($\gamma_r = 0, \gamma_a/g_r \in [0, 1]$, red solid curve), and the pure resonator dissipation case ($\gamma_a = 0, \gamma_r/g_r \in [0, 1]$, red dashed

curve), the statistics of $|\phi_{RR}|^2$ makes a transition from bunching to antibunching while the statistics of $|\phi_{LL}|^2$ (not plotted) remains antibunching throughout the scanning range. The case when both dissipations are present is not examined here as the left transmission dip disappears when $\gamma_a = \gamma_r \approx 0.6 g_r$. We have also investigated the scenarios when $\Gamma_r/g_r \neq 0.35$ but varies within the range $[0.1, 0.75]$, and identify qualitatively the same transition criteria.

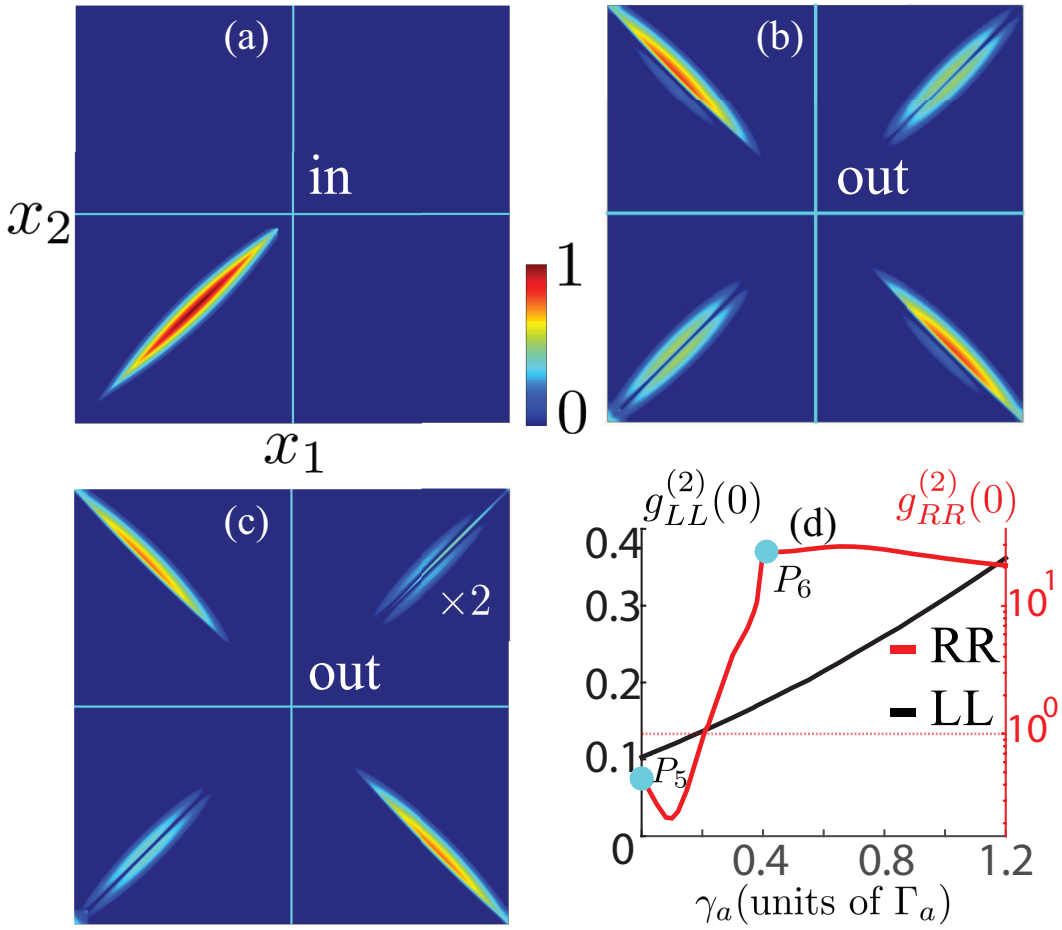

FIG. 5. Photonic correlations in the dissipative single-atom case with an entangled two-photon input. (a) Probability density of the incoming two-photon bound state. (b) Probability density of the scattered photons for $\gamma_a = 0$. (c) $\gamma_a = 0.4\Gamma_a$. Here, $|\phi_{RR}|^2$ (the probability density in Quadrant I) is multiplied by two to aid the visualization. (d) $g^{(2)}_{RR}(0)$ (red curve, right) and $g^{(2)}_{LL}(0)$ (black curve, left) for varying γ_a. The blue dots correspond to the cases in (b) and (c), respectively. The numerical values for one unit scale is (a) 0.11, (b) 0.03, and (c) 0.022, respectively.

Entangled two-photon input case. It is of great interest to investigate the effects of dissipations on the photonic correlation for an entangled two-photon input. Here, we con-

sider a special class of entangled inputs, *i.e.*, the two-photon bound state [26], which is a photonic bound state of two photons, and has been experimentally confirmed [5]. As illustrated in Fig. 5(a), the incoming bound state is represented by a wavefunction that is extended along $x_1 = x_2$, while is squeezed in the transverse direction. The functional form is given by $\phi_E = \exp[-\Gamma_a|x_1 - x_2|/v_g + i\omega_o(x_1 + x_2)/v_g - (x_1 - x_o)^2/4\sigma^2 - (x_2 - x_o)^2/4\sigma^2]$ ($\sigma\Gamma_a/v_g = 5, \omega_o = \omega_a,\ x_o/\sigma = -2.1$) [26]. When $\gamma_a = 0$, as shown in Fig. 5(b), the two transmitted photons (described by $|\phi_{RR}|^2$) and the two reflected photons (described by $|\phi_{LL}|^2$) are both antibunched [19]. When γ_a increases to $\approx 0.11\Gamma_a$, the statistics of $|\phi_{RR}|^2$ makes a transition from antibunching to bunching ($g^{(2)}_{RR}(0) \approx 0.22$). When γ_a is further increased, the statistics of $|\phi_{RR}|^2$ and $|\phi_{LL}|^2$ remains bunching and antibunching throughout the scanning range, respectively. Fig. 5(c) plots the case of a further increased $\gamma_a = 0.4\Gamma_a$, and Fig. 5(d) plots $g^{(2)}_{RR}(0)$ and $g^{(2)}_{LL}(0)$ as a function of γ_a. We have further investigated the class of inputs by generalizing ϕ_E so that the entanglement properties are different (see Appendix A for details). We find that for the class of inputs investigated, the transition in the RR branch now is changed from bunching to antibunching. The results indicate that the direction of the correlation transition depends on the entanglement of the input.

In this article, we computationally study the dissipation-induced correlation transition in wQED systems. Such a phenomenon may provide a recipe for the design of fundamental nodes of quantum-optical networks in the presence of dissipations [27, 28], and could tremendously enable the manipulation of photon entanglement [29] via dissipation-engineering techniques [30, 31]. Moreover, our results may also provide significant insights for studies on the effects of dissipations in quantum many-body systems [32].

This work was supported in part by NSF ECCS Grant No. 1608049.

Appendix A: Dynamics for various inputs and induced correlation transition

For the single-atom configuration, we examine the dynamics for various inputs to investigate the relation between the input states and the induced correlation transition. To begin with, we provide the information of the equations of motion. By applying the Schrödinger equation $i\hbar\partial_t|\Phi_a(t)\rangle = H_a|\Phi_a(t)\rangle$, and equating the coefficients for each basis, one obtains

$$
\begin{aligned}
\dot{\phi}_{RR}(x_1,x_2,t) &= -v_g(\partial_{x_1}+\partial_{x_2})\phi_{RR} - i\frac{V_a}{\sqrt{2}}[\delta(x_1)e_R(x_2,t)+\delta(x_2)e_R(x_1,t)]e^{-i\omega_a t},\\
\dot{\phi}_{RL}(x_1,x_2,t) &= -v_g(\partial_{x_1}-\partial_{x_2})\phi_{RL} - i\frac{V_a}{\sqrt{2}}[\delta(x_1)e_L(x_2,t)+\delta(x_2)e_R(x_1,t)]e^{-i\omega_a t},\\
\dot{\phi}_{LR}(x_1,x_2,t) &= v_g(\partial_{x_1}-\partial_{x_2})\phi_{LR} - i\frac{V_a}{\sqrt{2}}[\delta(x_1)e_R(x_2,t)+\delta(x_2)e_L(x_1,t)]e^{-i\omega_a t},\\
\dot{\phi}_{LL}(x_1,x_2,t) &= v_g(\partial_{x_1}+\partial_{x_2})\phi_{LL} - i\frac{V_a}{\sqrt{2}}[\delta(x_1)e_L(x_2,t)+\delta(x_2)e_L(x_1,t)]e^{-i\omega_a t},\\
\dot{e}_R(x,t) &= -v_g\partial_x e_R - \gamma_a e_R - i\frac{V_a}{\sqrt{2}}[\phi_{RR}(0,x,t)+\phi_{RR}(x,0,t)+\phi_{RL}(x,0,t)+\phi_{LR}(0,x,t)]e^{i\omega_a t},\\
\dot{e}_L(x,t) &= v_g\partial_x e_L - \gamma_a e_L - i\frac{V_a}{\sqrt{2}}[\phi_{LL}(0,x,t)+\phi_{LL}(x,0,t)+\phi_{LR}(x,0,t)+\phi_{RL}(0,x,t)]e^{i\omega_a t}.
\end{aligned}
\tag{A1}
$$

Using this set of equations of motion, we numerically evolve the dynamics and record the information of scattered photons for a specified dissipation rate γ_a. Then, we scan γ_a to investigate the correlation transitions and repeat such investigations for various inputs. In particular, the inputs can be classified into two types based upon their entanglement property, *i.e.*, the unentangled input (product state of single photons) and the entangled input (entangled state of photons). For the unentangled input, we first examine the Gaussian pulse (for both the resonance and the off-resonance cases), which is the typical optical excitation scheme for experiments. Moreover, motivated by the advent of wavefunction engineering technique, we further examine the pulse with a different functional form, *i.e.*, the resonant two-sided exponentially decaying pulse. Such a waveform is of interest as it has a higher single-photon and two-photon atomic excitation efficiency than the Gaussian pulse (see below). For the entangled input, we examine the two-photon bound state and a generalized bound state.

Here, we present the numerical results. For the Gaussian pulse to be resonant with the atom, we require the pulse duration to be much larger than the spontaneous emission time, *i.e.*, $\sigma\Gamma_a/v_g = 15$ so that $\sigma/v_g \gg 1/\Gamma_a$. Hereafter, for brevity, we shall use the time scale instead of the length scale to describe the photon waveform. The two quantities are connected by the relation, [length] = [time] $\times\, v_g$. To be specific, we take the spontaneous emission time $1/\Gamma_a = 1$ ns, and the Gaussian pulse duration is $2\sigma/v_g = 30$ ns. Here, the pulse duration is defined as the full width evaluated at which the single-photon probability density decays to $1/e$ of the maximal value. The numerical results have been discussed

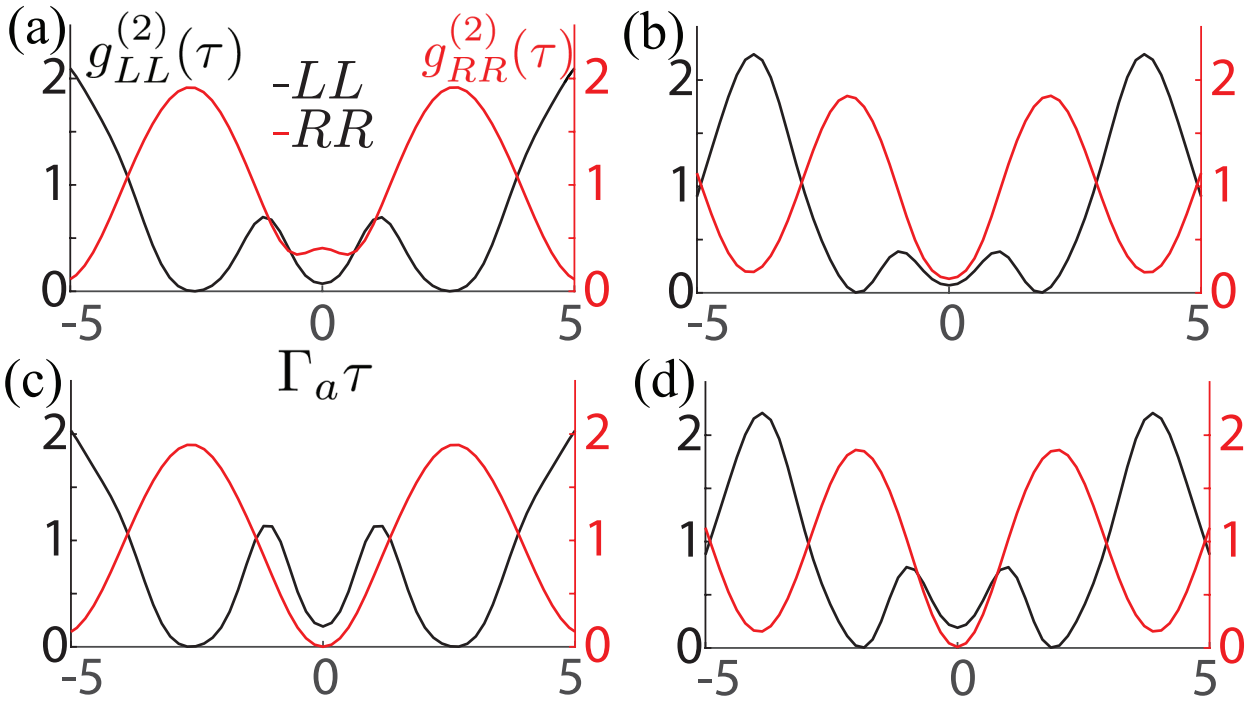

FIG. 6. $g^{(2)}(\tau)$ for the detuned Gaussian input in the single-atom case. (a) and (b) correspond to the case of $\omega_{01} = \omega_a + 0.6\Gamma_a, \omega_{02} = \omega_a - 0.6\Gamma_a$ for varying γ_a. (a) $\gamma_a = 0$. (b) $\gamma_a = 0.7\Gamma_a$. (c) and (d) correspond to the case of $\omega_{01} = \omega_a + 0.8\Gamma_a, \omega_{02} = \omega_a - 0.8\Gamma_a$ for varying γ_a. (c) $\gamma_a = 0$. (d) $\gamma_a = 0.7\Gamma_a$.

previously and presented in Fig. 3. For the off-resonant Gaussian input, we assume a special detuned Gaussian pulse wherein the center frequencies of two constituent photons, ω_{01} and ω_{02}, have opposite detuning with the atom (*i.e.*, $\omega_{01} = \omega_a + 0.6\Gamma_a, \omega_{02} = \omega_a - 0.6\Gamma_a$) while other parameters are the same as the resonant Gaussian pulse. We investigate such a pulse to understand the effect of the parameter space to deepen our understanding of the correlation transition. The correlation of scattered photons is shown in Fig. 6. When $\gamma_a = 0$, as shown in Fig. 6(a), $g^{(2)}_{RR}(\tau)$ (red curve) exhibits a peak around $\tau = 0$, indicating that two transmitted photons are bunched. $g^{(2)}_{LL}(\tau)$ (black curve) exhibits a dip around $\tau = 0$, indicating that two reflected photons are antibunched. When γ_a is varied in the range of $[0, \Gamma_a]$, the statistics of $|\phi_{RR}|^2$ undergoes a transition from bunching to antibunching at $\gamma_a \approx 0.1\Gamma_a$ while the statistics of $|\phi_{LL}|^2$ remains antibunching throughout the range. Fig. 6(b) plots the case for $\gamma_a = 0.7\Gamma_a$ wherein the $g^{(2)}_{RR}(0)$ now exhibits a dip, indicating photon antibunching statistics in the RR branch. We further investigate the correlation transitions when the detuning varies

in the range of $[0, \Gamma_a]$, and find that the correlation transition occurs only when the detuning is smaller than $0.7\Gamma_a$. For instance, when the detuning is $0.8\Gamma_a$ (*i.e.*, $\omega_{01} = \omega_a + 0.8\Gamma_a$ and $\omega_{02} = \omega_a - 0.8\Gamma_a$), the statistics of both $|\phi_{RR}|^2$ and $|\phi_{LL}|^2$ does not undergo a transition with a increasing γ_a. Fig. 6(c) and (d) plot the results for $\gamma_a = 0$ and $\gamma_a = 0.7\Gamma_a$, respectively, wherein the statistics of both $|\phi_{RR}|^2$ and $|\phi_{LL}|^2$ remains antibunching. In addition to the opposite detuning case, we also investigate the case when ω_{01} and ω_{02} have the same detuning in the range of $[0, \Gamma_a]$, and confirm qualitatively the same transition behavior from bunching to antibunching in the RR branch (not plotted).

For the resonant two-sided exponentially decaying pulse, each individual photon follows a two-sided exponentially decaying waveform of $\phi(x) = \sqrt{\Gamma_a/v_g}[e^{-\Gamma_a(x-x_o)/v_g}\theta(x - x_o) + e^{\Gamma_a(x-x_o)/v_g}\theta(x_o - x)]e^{i\omega_o x/v_g}$. $\theta(x)$ is the Heavistep function and $\omega_o = \omega_a$. $x_o \approx 4.95v_g/\Gamma_a$ is the center of the wavepacket, which has no relevance to our results as long as the initial position is far enough from the atom. Such a pulse can excite higher single-photon and two-photon atomic excitations than the aforementioned long Gaussian pulse because it has a bandwidth of Γ_a in a Lorentzian spectral line shape to match the atom-photon interaction bandwidth. Fig. 7(a) plots the incoming two-photon wavepacket, which resembles a diamond. When $\gamma_a = 0$, two transmitted photons (described by $|\phi_{RR}|^2$) are bunched while two reflected photons (described by $|\phi_{LL}|^2$) are antibunched, as shown in Fig. 7(b). Fig. 7(c) plots the corresponding $g^{(2)}(\tau)$ for both branches to confirm the photon statistics. When γ_a is varied in the range of $[0, \Gamma_a]$, the statistics of $|\phi_{RR}|^2$ undergoes a transition from bunching to antibunching at $\gamma_a \approx 0.4\Gamma_a$ while the statistics of $|\phi_{LL}|^2$ remains antibunching. Fig. 7(d) plots the scattered photons for $\gamma_a = 0.67\Gamma_a$, and Fig. 7(e) plots the corresponding $g^{(2)}(\tau)$, both indicating that the statistics of $|\phi_{RR}|^2$ now becomes antibunching.

For the entangled input, we first investigate the case for a two-photon bound state input ϕ_E. Specifically, the temporal scales of ϕ_E can be described by two quantities, *i.e.*, transverse and longitudinal durations, as shown in Fig. 8(a). The transverse duration (corresponding to the length perpendicular to the $x_1 = x_2$ axis) is determined by Γ_a, which is $1/(\sqrt{2}\Gamma_a) \approx 0.7$ ns (still adopting $1/\Gamma_a = 1$ ns). The longitudinal duration (corresponding to the length along the $x_1 = x_2$ axis) is determined by the Gaussian modulation, which is $2\sigma/v_g = 10$ ns. $\omega_o = \omega_a$ so that both photons are resonant with the atom. The initial position of the bound state is $x_o \approx -2.1\sigma$, and have no direct relevance to our numerical results. The numerical results have been discussed previously and shown in Fig. 5.

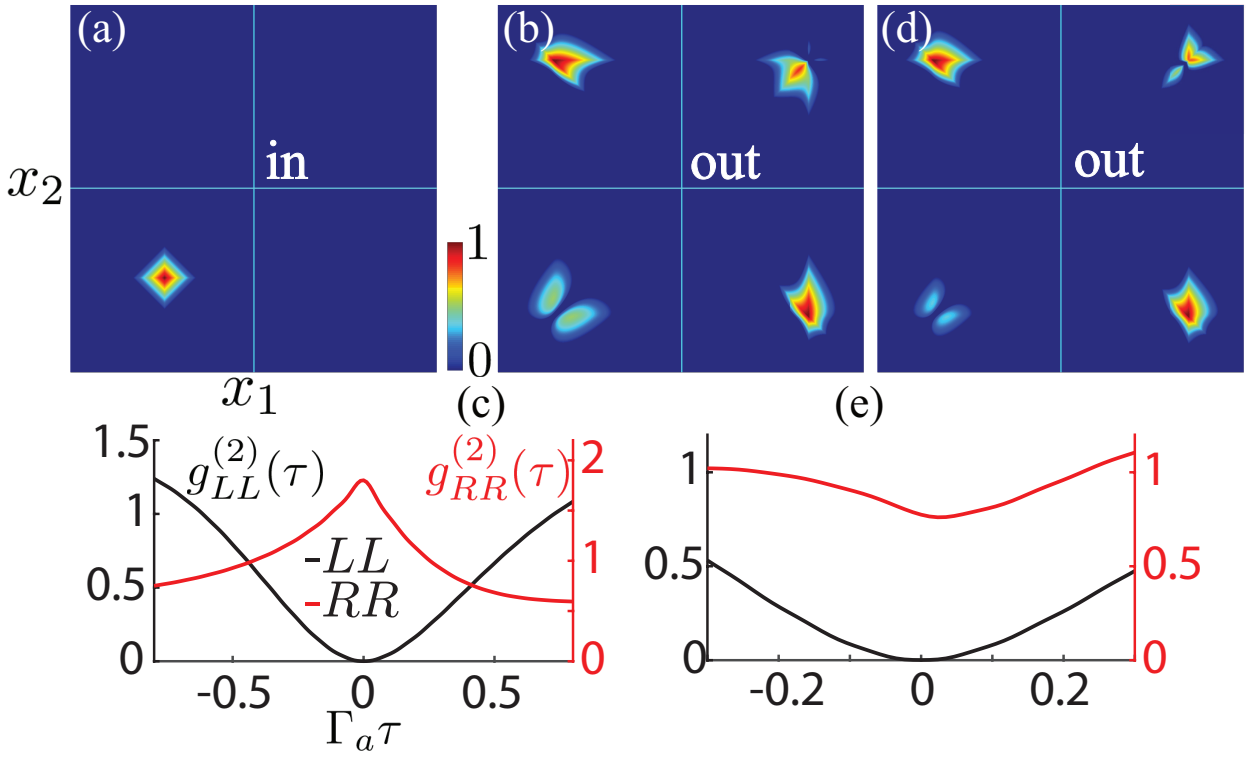

FIG. 7. Numerical results for the unentangled input of the resonant two-sided exponentially decaying pulse in the single-atom case. (a) Wavefunction density plot of the incoming wavepacket. (b) Wavefunction density plot of the scattered photons when $\gamma_a = 0$. (c) $g^{(2)}(\tau)$ of the scattered photons when $\gamma_a = 0$. (d) Wavefunction density plot of the scattered photons when $\gamma_a = 0.67\Gamma_a$. (e) $g^{(2)}(\tau)$ of the scattered photons when $\gamma_a = 0.67\Gamma_a$. The numerical values for one unit scale is (a) 0.022, (b) 0.0057, and (d) 0.0032, respectively.

We further investigate the case of a generalized form of the bound state, $\phi'_E = \exp[-\Gamma_a^m|x_1 - x_2|^m/v_g^m + i\omega_o(x_1+x_2)/v_g - (x_1-x_o)^2/4\sigma^2 - (x_2-x_o)^2/4\sigma^2]$ ($m = 2$, 3, and 4), using the same parameter set as ϕ_E. Here, we note that the incoming two photons are still bunched, but the input state now has a different transverse duration. In particular, the transverse duration is $\sqrt{2}/(2^{1/m}\Gamma_a)$ (*e.g.*, 1 ns, 1.12 ns, and 1.19 ns for $m = 2$, 3, and 4, respectively) while other temporal properties of ϕ'_E are the same as ϕ_E. We first examine the case when the input is $\phi_{E'}$ for $m = 2$. As shown in Fig. 8(b), when $\gamma_a = 0$, two transmitted photons (described by $|\phi_{RR}|^2$) are bunched while two reflected photons (described by $|\phi_{LL}|^2$) are antibunched. We now vary γ_a in the range of $[0, \Gamma_a]$, and observe that the statistics of $|\phi_{RR}|^2$ undergoes a transition from bunching to antibunching at $\gamma_a \approx 0.6\Gamma_a$ while the statistics of

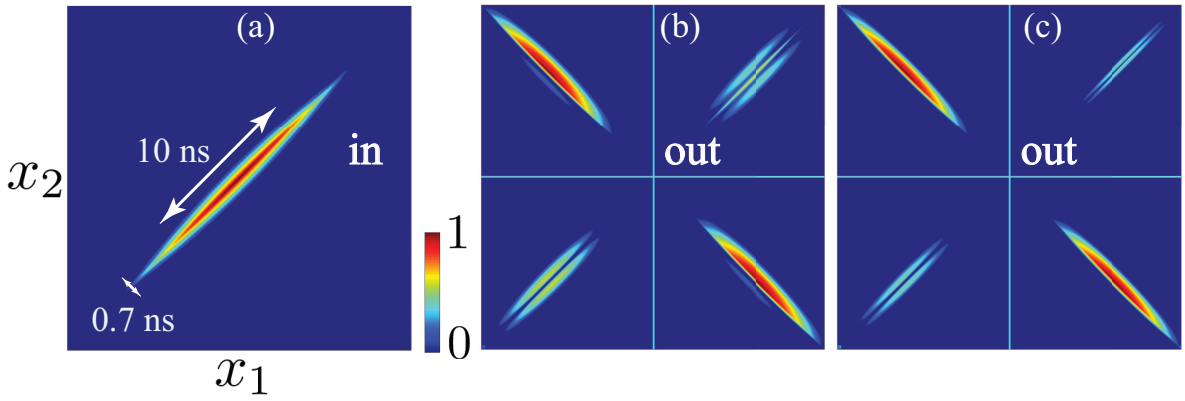

FIG. 8. Wavefunction density plot. (a) The incoming two-photon bound state $|\phi_E|^2$. (b) and (c) plot the scattered photons for the entangled input ϕ'_E ($m = 2$) with varying γ_a. (b) When $\gamma_a = 0$. (c) When $\gamma_a = 0.7\Gamma_a$. The numerical values for each unit scale is (a) 0.11, (b) 0.027, and (c) 0.014, respectively.

$|\phi_{LL}|^2$ remains antibunching throughout the scanning range. Fig. 8(c) plots the scattered photons for $\gamma_a = 0.7\Gamma_a$ wherein both transmitted and reflected photons are antibunched. For the cases of $m = 3$ and $m = 4$, we observe qualitatively the same transition behaviors, both occurring at $\gamma_a \approx 0.5\Gamma_a$ (not shown).

Here, we summarize the relation between the input state and the induced correlation transition, as illustrated in Fig. 9. Based upon the inputs investigated, we draw the following conclusions. For the unentangled input case, we have examined the resonant, off-resonant Gaussian pulses, and the resonant two-sided exponentially decaying pulse to confirm that the transition only occurs in the RR branch from bunching to antibunching. The transition from antibunching to bunching is not observed. For the entangled input case, we confirm the correlation transitions for both the two-photon bound state ϕ_E and the generalized bound state ϕ'_E in the RR branch whereas the direction is different. The transition direction for ϕ_E is from antibunching to bunching whereas from bunching to antibunching for ϕ'_E.

Appendix B: Equations of motion for atom-cavity configuration

For the atom-cavity configuration (Fig. 1(b)), we provide the information of the Hamiltonian, the general state, and the equations of motion. The reduced Hamiltonian describing

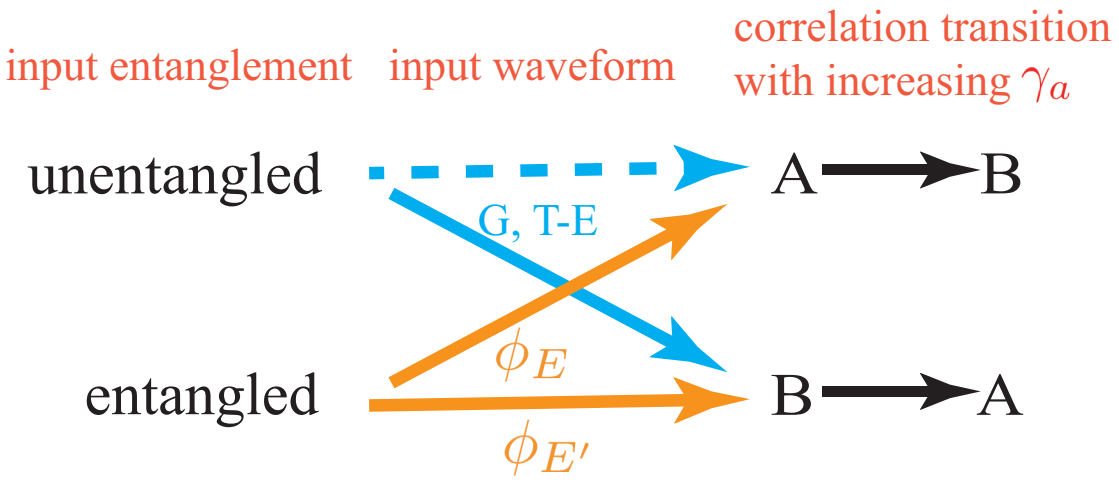

FIG. 9. Illustration of the relation between the input state and the induced correlation transition. The abbreviations represent, A: antibunching; B: bunching; G: resonant and off-resonant Gaussian pulses; and T-E: resonant two-sided exponentially decaying input. ϕ_E and $\phi_{E'}$ are the two-photon bound state and the generalized bound state, respectively. The non-black solid arrows indicate that the correlation transitions have been numerically confirmed for particular types of input that are specified by the abbreviations and variables. The non-black dashed arrow indicates that the correlation transition from antibunching to bunching for the unentangled input is not observed. The black arrows denote the direction of the induced correlation transition.

such a system, H_c, is described by

$$\begin{aligned}\frac{H_c}{\hbar} = \int dx \Big(& c_R^\dagger(x)(-iv_g\partial_x)c_R(x) + c_L^\dagger(x)(iv_g\partial_x)c_L(x) \\ & + V_c\delta(x)\left[(c_R^\dagger(x)+c_L^\dagger(x))c + c^\dagger(c_R(x)+c_L(x))\right]\Big) \\ & + (\omega_c - i\gamma_c)c^\dagger c + (\omega_e - i\gamma_a)a_e^\dagger a_e + \omega_g a_g^\dagger a_g \\ & + g_c(c^\dagger\sigma_- + \sigma_+ c),\end{aligned} \tag{B1}$$

where $c^\dagger$ (c) denotes the creation (annihilation) operator for the cavity mode. V_c is the cavity-photon coupling strength ($V_c^2/v_g \equiv \Gamma_c$ is the cavity decay rate into the waveguide). g_c is the atom-cavity coupling strength. The notations regarding the waveguided photon and the atom are defined the same as those in the single-atom configuration. The general state of the restricted system, $|\Phi_c(t)\rangle$, is

$$|\Phi_c(t)\rangle = \Big(\int dx \sum_{j=R,L} e_{aj}(x,t) c_j^\dagger(x) e^{-i\omega_e t} \sigma_+ + \int dx \sum_{j=R,L} e_{cj}(x,t) c_j^\dagger(x) e^{-i(\omega_g+\omega_c)t} c^\dagger$$
$$+ \iint dx_1 dx_2 \sum_{j,l=R,L} \phi_{jl}(x_1,x_2,t) e^{-i\omega_g t} \frac{c_j^\dagger(x_1) c_l^\dagger(x_2)}{\sqrt{2}} + e_{cc}(t) e^{-i(2\omega_c+\omega_g)t} \frac{1}{\sqrt{2}} c^\dagger c^\dagger + e_{ac}(t) e^{-i(\omega_e+\omega_c)t} c^\dagger \sigma_+ \Big) |\varnothing\rangle, \tag{B2}$$

where $e_{aR(L)}$ denotes the single-photon probability amplitude wherein one photon is absorbed by the atom and the other waveguided photon is moving to the right (left). $e_{cR(L)}$ denotes the single-photon probability amplitude wherein one photon excites the cavity mode and the other waveguided photon is moving to the right (left). e_{cc} is the cavity excitation amplitude wherein both photons excite the cavity mode. e_{ac} represents the excitation amplitude wherein one photon is absorbed by the atom and the other photon excites the cavity mode. Two-photon wavefunctions ϕ_{RR}, ϕ_{RL}, ϕ_{LR}, and ϕ_{LL} are defined the same as the single-atom case. By applying the Schrödinger equation $i\hbar\partial_t|\Phi_c(t)\rangle = H_c|\Phi_c(t)\rangle$, one determines the following equations of motion,

$$\dot{\phi}_{RR}(x_1,x_2,t) = -v_g(\partial_{x_1}+\partial_{x_2})\phi_{RR} - i\frac{V_c}{\sqrt{2}}[\delta(x_1)e_{cR}(x_2,t)+\delta(x_2)e_{cR}(x_1,t)]e^{-i\omega_c t},$$
$$\dot{\phi}_{RL}(x_1,x_2,t) = -v_g(\partial_{x_1}-\partial_{x_2})\phi_{RL} - i\frac{V_c}{\sqrt{2}}[\delta(x_1)e_{cL}(x_2,t)+\delta(x_2)e_{cR}(x_1,t)]e^{-i\omega_c t},$$
$$\dot{\phi}_{LR}(x_1,x_2,t) = v_g(\partial_{x_1}-\partial_{x_2})\phi_{LR} - i\frac{V_c}{\sqrt{2}}[\delta(x_1)e_{cR}(x_2,t)+\delta(x_2)e_{cL}(x_1,t)]e^{-i\omega_c t},$$
$$\dot{\phi}_{LL}(x_1,x_2,t) = v_g(\partial_{x_1}+\partial_{x_2})\phi_{LL} - i\frac{V_c}{\sqrt{2}}[\delta(x_1)e_{cL}(x_2,t)+\delta(x_2)e_{cL}(x_1,t)]e^{-i\omega_c t},$$
$$\dot{e}_{cR}(x,t) = -v_g\partial_x e_{cR} - \gamma_c e_{cR} - i\frac{V_c}{\sqrt{2}}[\phi_{RR}(0,x,t)+\phi_{RR}(x,0,t)+\phi_{RL}(x,0,t)+\phi_{LR}(0,x,t)]e^{i\omega_c t}$$
$$- i\sqrt{2}V_c\delta(x)e_{cc}(t)e^{-i\omega_c t} - ig_c e_{aR}(x,t)e^{-i\Delta_1 t},$$
$$\dot{e}_{cL}(x,t) = v_g\partial_x e_{cL} - \gamma_c e_{cL} - i\frac{V_c}{\sqrt{2}}[\phi_{LL}(0,x,t)+\phi_{LL}(x,0,t)+\phi_{LR}(x,0,t)+\phi_{RL}(0,x,t)]e^{i\omega_c t}$$
$$- i\sqrt{2}V_c\delta(x)e_{cc}(t)e^{-i\omega_c t} - ig_c e_{aL}(x,t)e^{-i\Delta_1 t},$$
$$\dot{e}_{aR}(x,t) = -v_g\partial_x e_{aR} - \gamma_a e_{aR} - iV_c\delta(x)e_{ac}(t)e^{-i\omega_c t} - ig_c e_{cR}(x,t)e^{i\Delta_1 t},$$
$$\dot{e}_{aL}(x,t) = v_g\partial_x e_{aL} - \gamma_a e_{aL} - iV_c\delta(x)e_{ac}(t)e^{-i\omega_c t} - ig_c e_{cL}(x,t)e^{i\Delta_1 t},$$
$$\dot{e}_{cc}(t) = -2\gamma_c e_{cc} - i\sqrt{2}V_c[e_{cR}(0,t)+e_{cL}(0,t)]e^{i\omega_c t} - i\sqrt{2}g_c e_{ac}(t)e^{-i\Delta_1 t},$$
$$\dot{e}_{ac}(t) = -(\gamma_a+\gamma_c)e_{ac} - iV_c[e_{aR}(0,t)+e_{aL}(0,t)]e^{i\omega_c t} - i\sqrt{2}g_c e_{cc}(t)e^{i\Delta_1 t},$$
(B3)

where $\Delta_1 = \omega_a - \omega_c$ describes the frequency detuning between the atom and the cavity mode. More information about the numerical work can be found in Ref. [24]

Appendix C: Equations of motion for atom-ring-resonator configuration

For the atom-ring-resonator configuration (Fig. 1(c)), we now provide the information of the Hamiltonian, the general state, and the equations of motion. The reduced Hamiltonian describing such a system, H_r, is described by

$$\begin{aligned}\frac{H_r}{\hbar} = &\int dx\Big(c_R^\dagger(x)(-iv_g\partial_x)c_R(x) + c_L^\dagger(x)(iv_g\partial_x)c_L(x)\\ &+V_r\delta(x)\left[c_R^\dagger(x)a + a^\dagger c_R(x) + c_L^\dagger(x)b + b^\dagger c_L(x)\right]\Big)\\ &+(\omega_r - i\gamma_r)a^\dagger a + (\omega_r - i\gamma_r)b^\dagger b + (\omega_e - i\gamma_a)a_e^\dagger a_e\\ &+\omega_g a_g^\dagger a_g + g_r(a^\dagger\sigma_- + \sigma_+ a) + g_r(b^\dagger\sigma_- + \sigma_+ b).\end{aligned} \tag{C1}$$

In particular, the ring-resonator supports two degenerate counter-propagating modes, *i.e.*, counter-clockwise (CCW) and the clockwise (CW) modes. $a^\dagger$ (a) and $b^\dagger$ (b) are the creation (annihilation) operators for the CCW and CW modes, respectively. V_r denotes the atom-resonator coupling strength ($V_r^2/2v_g \equiv \Gamma_r$ is the resonator decay rate into the waveguide [25]). To illustrate the physics, we assume a perfect ring-resonator wherein both propagating modes have the same resonant frequency ω_r, the same dissipation rate γ_r, the same atom-resonator coupling strength g_r, and no inter-mode coupling is taken into account. The notations regarding the waveguided photon and the atom are defined the same as those in the single-atom configuration. The general state of the restricted system, $|\Phi_r(t)\rangle$, is

$$\begin{aligned}|\Phi_r(t)\rangle = &\Big(\int dx\sum_{j=R,L} e_{Aj}(x,t)c_j^\dagger(x)e^{-i\omega_e t}\sigma_+ + \int dx\sum_{j=R,L} e_{aj}(x,t)c_j^\dagger(x)e^{-i(\omega_g+\omega_c)t}a^\dagger\\ &+\int dx\sum_{j=R,L} e_{bj}(x,t)c_j^\dagger(x)e^{-i(\omega_g+\omega_c)t}b^\dagger + \iint dx_1dx_2\sum_{j,l=R,L}\phi_{jl}(x_1,x_2,t)e^{-i\omega_g t}\frac{c_j^\dagger(x_1)c_l^\dagger(x_2)}{\sqrt{2}}\\ &+e_{aa}(t)e^{-i(2\omega_c+\omega_g)t}\frac{1}{\sqrt{2}}a^\dagger a^\dagger + e_{bb}(t)e^{-i(2\omega_c+\omega_g)t}\frac{1}{\sqrt{2}}b^\dagger b^\dagger + e_{ab}(t)e^{-i(2\omega_c+\omega_g)t}a^\dagger b^\dagger\\ &+e_{aA}(t)e^{-i(\omega_e+\omega_c)t}a^\dagger\sigma_+ + e_{bA}(t)e^{-i(\omega_e+\omega_c)t}b^\dagger\sigma_+\Big)|\varnothing\rangle,\end{aligned} \tag{C2}$$

where $e_{AR(L)}$ denotes the single-photon probability amplitude when one photon is absorbed by the atom and the other waveguided photon is moving to the right (left). $e_{aR(L)}$ denotes

the single-photon probability amplitude wherein one photon excites the CCW mode and the other waveguided photon is moving to the right (left). $e_{bR(L)}$ denotes the single-photon probability amplitude wherein one photon excites the CW mode and the other waveguided photon is moving to the right (left). e_{aa} (e_{bb}) is the excitation amplitude wherein both photons excite the CCW (CW) mode. e_{ab} is the excitation amplitude wherein two photons excite the CWW and CW modes, respectively. e_{aA} (e_{bA}) denotes the excitation amplitude wherein one photon is absorbed by the atom while the other photon excites the CCW (CW) mode. Two-photon wavefunctions ϕ_{RR}, ϕ_{RL}, ϕ_{LR}, and ϕ_{LL} are defined the same as the single-atom case. By applying the Schrödinger equation $i\hbar\partial_t|\Phi_r(t)\rangle = H_r|\Phi_r(t)\rangle$, one determines the following equations of motion,

$$
\begin{aligned}
&\dot{\phi}_{RR}(x_1,x_2,t) = -v_g(\partial_{x_1}+\partial_{x_2})\phi_{RR} - i\frac{V_r}{\sqrt{2}}[\delta(x_1)e_{aR}(x_2,t)+\delta(x_2)e_{aR}(x_1,t)]e^{-i\omega_c t},\\
&\dot{\phi}_{RL}(x_1,x_2,t) = -v_g(\partial_{x_1}-\partial_{x_2})\phi_{RL} - i\frac{V_r}{\sqrt{2}}[\delta(x_1)e_{aL}(x_2,t)+\delta(x_2)e_{bR}(x_1,t)]e^{-i\omega_c t},\\
&\dot{\phi}_{LR}(x_1,x_2,t) = v_g(\partial_{x_1}-\partial_{x_2})\phi_{LR} - i\frac{V_r}{\sqrt{2}}[\delta(x_1)e_{bR}(x_2,t)+\delta(x_2)e_{aL}(x_1,t)]e^{-i\omega_c t},\\
&\dot{\phi}_{LL}(x_1,x_2,t) = v_g(\partial_{x_1}+\partial_{x_2})\phi_{LL} - i\frac{V_r}{\sqrt{2}}[\delta(x_1)e_{bL}(x_2,t)+\delta(x_2)e_{bL}(x_1,t)]e^{-i\omega_c t},\\
&\dot{e}_{aR}(x,t) = -v_g\partial_x e_{aR} - \gamma_c e_{aR} - i\frac{V_r}{\sqrt{2}}[\phi_{RR}(0,x,t)+\phi_{RR}(x,0,t)]e^{i\omega_c t} - i\sqrt{2}V_r\delta(x)e_{aa}(t)e^{-i\omega_c t}\\
&- ig_r e_{AR}(x,t)e^{-i\Delta_2 t},\\
&\dot{e}_{bR}(x,t) = -v_g\partial_x e_{bR} - \gamma_c e_{bR} - i\frac{V_r}{\sqrt{2}}[\phi_{RL}(x,0,t)+\phi_{LR}(0,x,t)]e^{i\omega_c t} - iV_r\delta(x)e_{ab}(t)e^{-i\omega_c t}\\
&- ig_r e_{AR}(x,t)e^{-i\Delta_2 t},\\
&\dot{e}_{aL}(x,t) = v_g\partial_x e_{aL} - \gamma_c e_{aL} - i\frac{V_r}{\sqrt{2}}[\phi_{RL}(0,x,t)+\phi_{LR}(x,0,t)]e^{i\omega_c t} - iV_r\delta(x)e_{ab}(t)e^{-i\omega_c t}\\
&- ig_r e_{AL}(x,t)e^{-i\Delta_2 t},\\
&\dot{e}_{bL}(x,t) = v_g\partial_x e_{bL} - \gamma_c e_{bL} - i\frac{V_r}{\sqrt{2}}[\phi_{LL}(x,0,t)+\phi_{LL}(0,x,t)]e^{i\omega_c t} - i\sqrt{2}V_r\delta(x)e_{bb}(t)e^{-i\omega_c t}\\
&- ig_r e_{AL}(x,t)e^{-i\Delta_2 t},\\
&\dot{e}_{AR}(x,t) = -v_g\partial_x e_{AR} - \gamma_a e_{AR} - iV_r\delta(x)e_{aA}(t)e^{-i\omega_c t} - ig_r[e_{aR}(x,t)+e_{bR}(x,t)]e^{i\Delta_2 t},\\
&\dot{e}_{AL}(x,t) = v_g\partial_x e_{AL} - \gamma_a e_{AL} - iV_r\delta(x)e_{bA}(t)e^{-i\omega_c t} - ig_r[e_{aL}(x,t)+e_{bL}(x,t)]e^{i\Delta_2 t},\\
&\dot{e}_{aa}(t) = -2\gamma_c e_{cc} - i\sqrt{2}V_r e_{aR}(0,t)e^{i\omega_c t} - i\sqrt{2}g_r e_{aA}(t)e^{-i\Delta_2 t},\\
&\dot{e}_{bb}(t) = -2\gamma_c e_{bb} - i\sqrt{2}V_r e_{bL}(0,t)e^{i\omega_c t} - i\sqrt{2}g_r e_{bA}(t)e^{-i\Delta_2 t},\\
&\dot{e}_{ab}(t) = -2\gamma_c e_{ab} - iV_r[e_{bR}(0,t)+e_{aL}(0,t)]e^{i\omega_c t} - ig_r[e_{bA}(t)+e_{aA}(t)]e^{-i\Delta_2 t},\\
&\dot{e}_{aA}(t) = -(\gamma_a+\gamma_c)e_{aA} - iV_r e_{AR}(0,t)e^{i\omega_c t} - i\sqrt{2}g_r e_{aa}(t)e^{i\Delta_2 t} - ig_r e_{ab}(t)e^{i\Delta_2 t},\\
&\dot{e}_{bA}(t) = -(\gamma_a+\gamma_c)e_{bA} - iV_r e_{AL}(0,t)e^{i\omega_c t} - i\sqrt{2}g_r e_{bb}(t)e^{i\Delta_2 t} - ig_r e_{ab}(t)e^{i\Delta_2 t},
\end{aligned}
\tag{C3}
$$

where $\Delta_2 = \omega_a - \omega_r$ describes the detuning between the atom and the resonator mode. More information about the numerical work can be found in Ref. [21].

[1] L. Davidovich, M. Brune, J. M. Raimond, and S. Haroche, Phys. Rev. A **53**, 1295 (1996).

[2] M. Neeley, M. Ansmann, R. C. Bialczak, M. Hofheinz, N. Katz, E. Lucero, A. O'Connell, H. Wang, A. N. Cleland, and J. M. Martinis, Phys. Rev. B **77**, 180508 (2008).

[3] Y. Zhou, Z. Chen, and J.-T. Shen, Phys. Rev. A **95**, 043832 (2017).

[4] A. Imamoḡlu, H. Schmidt, G. Woods, and M. Deutsch, Phys. Rev. Lett. **79**, 1467 (1997).

[5] O. Firstenberg, T. Peyronel, Q.-Y. Liang, A. V. Gorshkov, M. D. Lukin, and V. Vuletic, Nature **502**, 71 (2013).

[6] Y. Shen and J.-T. Shen, Phys. Rev. A **92**, 033803 (2015).

[7] C. J. Hood, M. S. Chapman, T. W. Lynn, and H. J. Kimble, Phys. Rev. Lett. **80**, 4157 (1998).

[8] J. Eschner, C. Raab, F. Schmidt-Kaler, and R. Blatt, Nature **413**, 495 (2001).

[9] A. Wallraff, D. I. Schuster, A. Blais, L. Frunzio, R.-S. Huang, J. Majer, S. Kumar, S. M. Girvin, and R. J. Schoelkopf, Nature **431**, 162 (2004).

[10] I. Fushman, D. Englund, A. Faraon, N. Stoltz, P. Petroff, and J. Vučković, Science **320**, 769 (2008).

[11] K. M. Birnbaum, A. Boca, R. Miller, A. D. Boozer, T. E. Northup, and H. J. Kimble, Nature **436**, 87 (2005).

[12] K. Hennessy, A. Badolato, M. Winger, D. Gerace, M. Atature, S. Gulde, S. Falt, E. L. Hu, and A. Imamoglu, Nature **445**, 896 (2007).

[13] T. Aoki, B. Dayan, E. Wilcut, W. P. Bowen, A. S. Parkins, T. J. Kippenberg, K. J. Vahala, and H. J. Kimble, Nature **443**, 671 (2006).

[14] K. Srinivasan and O. Painter, Nature **450**, 862 (2007).

[15] J.-T. Shen and S. Fan, Phys. Rev. A **76**, 062709 (2007).

[16] J.-T. Shen and S. Fan, Phys. Rev. A **79**, 023837 (2009).

[17] Z. Chen, Y. Zhou, and J.-T. Shen, Opt. Lett. **42**, 887 (2017).

[18] M. Bradford and J.-T. Shen, Opt. Lett. **39**, 5558 (2014).

[19] See Supplemental Material at for the animations of the scattering processes for the resonant Gaussian input when $\gamma_a = 0, 0.85\Gamma_a$, and the bound state input when $\gamma_a = 0$.

[20] The criteria for photonic bunching and antibunching are given by $g^{(2)}(\tau) < g^{(2}(0)$ and $g^{(2)}(\tau) > g^{(2}(0)$, respectively, see M. O. Scully and M. S. Zubairy, *Quantum optics* (Cambridge university press, 1997) p. 135.

[21] Z. Chen, Y. Zhou, and J.-T. Shen, Opt. Lett. **41**, 3313 (2016).

[22] O. Astafiev, A. M. Zagoskin, A. A. Abdumalikov, Y. A. Pashkin, T. Yamamoto, K. Inomata, Y. Nakamura, and J. S. Tsai, Science **327**, 840 (2010).

[23] J. M. Martinis, S. Nam, J. Aumentado, and C. Urbina, Phys. Rev. Lett. **89**, 117901 (2002).

[24] M. Bradford and J.-T. Shen, Phys. Rev. A **92**, 023810 (2015).

[25] J.-T. Shen and S. Fan, Phys. Rev. A **79**, 023838 (2009).

[26] J.-T. Shen and S. Fan, Phys. Rev. Lett. **98**, 153003 (2007).

[27] H. J. Kimble, Nature **453**, 1023 (2008).

[28] A. Sipahigil, R. E. Evans, D. D. Sukachev, M. J. Burek, J. Borregaard, M. K. Bhaskar, C. T. Nguyen, J. L. Pacheco, H. A. Atikian, C. Meuwly, R. M. Camacho, F. Jelezko, E. Bielejec, H. Park, M. Lončar, and M. D. Lukin, Science **354**, 847 (2016).

[29] F. Quijandría, D. Porras, J. J. García-Ripoll, and D. Zueco, Phys. Rev. Lett. **111**, 073602 (2013).

[30] J. F. Poyatos, J. I. Cirac, and P. Zoller, Phys. Rev. Lett. **77**, 4728 (1996).

[31] K. W. Murch, U. Vool, D. Zhou, S. J. Weber, S. M. Girvin, and I. Siddiqi, Phys. Rev. Lett. **109**, 183602 (2012).

[32] F. Brennecke, R. Mottl, K. Baumann, R. Landig, T. Donner, and T. Esslinger, Proceedings of the National Academy of Sciences **110**, 11763 (2013).